Processing and Application of Ceramics 17 [3] (2023) 248–255
https://doi.org/10.2298/PAC2303248Z

Fluorine substituted hydroxyapatite microspheres: Template-free hydrothermal synthesis and sustained fluoride-releasing properties

Qing-Xia Zhu[1,*], Li Liu[1], Wan-Ting Xu[2], Quan-Yi Nie[3], Yun-Long Xu[1], Jia-Xin Liu[1]

[1]*Tianjin Key Laboratory of Advanced Fibers and Energy Storage, School of Material Science and Engineering, Tiangong University, Tianjin 300387, China*
[2]*North China University of Technology, Beijing 100144, China*
[3]*Chaozhou Sanhuan Ceramic Co. Ltd, Guangdong 515646,China*

Received 11 February 2023; Received in revised form 6 June 2023; Accepted 1 July 2023

Abstract

To avoid sudden release of fluoride, F-substituted hydroxyapatite (FHA) porous microspheres were prepared for the treatment of F-deficiency tissues. In the absence of any template-directing reagents, FHA microspheres with diameters of about 30 μm were successfully fabricated via hydrothermal method with urea as homogeneous precipitant to regulate the nucleation, growth and self-assembly process. Urea concentration and hydrothermal temperature played an important role in the formation and regulation of spherical hydroxyapatite. The synthesized FHA microspheres with large specific surface area, large pore volume and complex porous structure were efficient for the adsorption and long-term stable release of ionic extracts. Concentration of F^- ions in physiological salt solution was maintained in the range of the therapeutic window without exceeding the toxic threshold within 30 days. The ionic extracts of FHA porous microspheres promoted the proliferation of human osteoblast-like cells (MG-63). The fabricated FHA microspheres may be a potential candidate as bioactive fluoride-release carriers for the treatment of osteoporosis and bone defects.

Keywords: *porous hydroxyapatite, microspheres, hydrothermal method, self-assembly, fluoride-releasing*

I. Introduction

Fluorine mainly exists in hard tissues, such as bones and teeth as an essential trace element. Fluoride ion has attracted attention due to its therapeutic ability in osteoporosis. Supplemental F^-, upon implantation in a bone substitute, promotes bone formation around the implant and accelerates the recovery process in elderly people. Fluoride-containing substances, such as highly soluble sodium fluoride, calcium fluoride and sodium monofluorophosphate, are usually combined with organic carriers (such as composite resin [1], oligomeric L-lactic acid [2], glass ionomer cement [3], sodium alginate [4], hydroxymethyl chitosan [5], etc.) to prepare fluoride sustained-release materials. However, the above-mentioned highly soluble fluoride and strong biodegradable carrier can easily cause the sudden and excess release of fluoride [6]. In addition, during the treatment of bone diseases, organic carriers cannot have the dual functions of nidus filling and drug release.

Common inorganic bioactive carriers [7] include bioglass, calcium phosphate and hydroxyapatite (HA). However, the loss of introduced fluoride during the melting process and the high dissolution rate of bioglass limit its long-term stability. Fluoride ions cannot enter the calcium phosphate structure and are often enriched at the grain boundary, which easily leads to sudden release of fluoride. Hydroxyapatite has good biocompatibility and can be slowly dissolved in the body. Unlike the physical adsorption, hydrogen bond or electrostatic adsorption between HA and other drugs, fluoride can enter the apatite lattice to form fluoride substituted apatite (FHA). So far, the effect of F^- ions on HA structure and properties has been widely reported. F-substitution not only changes the composition, solubility and crystallinity of HA, but also is important in cell proliferation, bone development and has pharmaceutical effects on bone regeneration [8–10]. FHA has improved crystallinity and markedly reduced acid reactivity, exhibits superior corrosion resistance, biocompatibility and chemical stability. A local release of F^- ions

*Corresponding author: tel: +86 13879889568,
e-mail: *zhuqingxia@tiangong.edu.cn*

in a low dosage may improve bone regeneration, avoiding the sudden release of fluoride at the initial stage. Thus, it has aroused widespread interest for FHA and *in situ* sustained-release of ionic extracts for the treatment of osteoporosis.

The regular porous HA microsphere material has the advantages of high specific surface area, good affinity and excellent adsorption ability. Moreover, the adsorbed ions can achieve uniform and equal release from all sides. Thus, spherical HA has promising applications for bone/tooth materials as bioactive carrier. It has attracted widespread attention in the field of drug sustained release. Conventional precipitated HA often shows rod-shaped aggregates because of the preferred orientation growth of HA crystal along the c-axis. The traditional strategy to synthesize porous microspheres is focused on the template method. Porous HA microspheres are self-assembled by electrostatic interaction between organic polymers spherical micelles and HA nanosheets [11,12]. Inorganic or organic solid microspheres can also be used as templates to form HA microspheres by heterogeneous nucleation or ion exchange [13]. These methods require the sacrifice of templates, which may be harmful to health and environment. Up to now, self-assembly of microspheres in the absence of any templates is still a major challenge. At the low-temperature hydrothermal conditions, hydrolysis of homogeneous precipitant generates the driving force for crystal nucleation, growth and self-assembly process, thus controlling the morphology and structure. Hydrothermal reaction has become the common method to prepare spherical structures. The similar phenomenon of nucleation-dissolution-recrystallization-self-assembly growth process has been widely observed in the synthesis of metal oxides and other kinds of materials [14]. However, further work needs to be done to understand the role of all parameters in structure regulation, such as concentration, pH value and hydrothermal temperature. Up to now, lots of studies have focused on the effect of hydrothermal conditions on the grain size and morphology [15], and the effects on the self-assembly process of microspheres are rarely reported.

In the present study, FHA microspheres with porous structure via hydrothermal process have been developed. The effects of urea concentrations and hydrothermal temperature on the crystal structure, morphology and self-assembly process of FHA microspheres were further investigated. The sustained release of fluoride ions and osteoblast cell (MG-63) proliferation were evaluated to lay the foundation for the treatment of osteogenic disease.

II. Experimental details

2.1. Synthesis and characterization

All chemicals $Ca(NO_3)_2 \cdot 4\,H_2O$, $(NH_4)_2HPO_4$, NH_4F were analytical grade reagents obtained from Tianjin Fengchuan Chemical Reagent Technology Co. Ltd. and used without further purification. In the synthesis process, the aqueous solutions containing 0.15 mol/l Ca^{2+}, 0.09 mol/l HPO_4^{2-} and 0.01 mol/l F^- were added drop-wise into the urea solution with designed molar concentrations of 0.75, 1, 1.25 and 1.50 mol/l. Correspondingly, the obtained products were labelled as U1, U2, U3 and U4, respectively. A solution of 0.1 mol/l HNO_3 was used to adjust pH to 2.50–2.55 to obtain clear solutions. Then 70 ml of the obtained solution was transferred into 90 ml autoclave and heated at certain temperature (90, 120 or 150 °C) for 48 h, followed by cooling to room temperature naturally. Finally, the obtained suspension was filtered and washed with distilled water and anhydrous ethanol for three times. The obtained powders were dried at 120 °C for 24 h.

The structures of the samples were investigated by X-ray diffraction (XRD, D8 Advance, Bruker, Germany) with monochromatic Cu Kα radiation. The lattice constants were calculated from the well determined positions of the intense XRD diffraction peaks that were processed by MDI Jade 6.1 software. To evaluate the crystallinity degree, the reflection of the (211) plane of the pure HA was selected for crystallinity measurement and calculation of the relative index of crystallinity. The morphology and particle size of the samples were determined by scanning electron microscopy (SEM, JSM-6700F, JEOL, Japan). Nitrogen adsorption and desorption was used to analyse the specific surface area and pore size of the samples (BET, BELSORP-max, MicrotraBEL, Japan). Fluoride contents in the apatite were quantified by X-ray fluorescence spectroscopy (XFS, ARLADVANT'X IntelliPower TM, Thermofisher, USA).

2.2. Fluoride ion release test

200 mg of the FHA microspheres was placed into 100 ml of physiological solution and allowed to stay at 37 °C. After certain periods of time, the physiological solution was filtered using a membrane with a pore size of 0.22 μm, and the F^- concentration in the solution was measured by Fluoride ion meter (D-53, Horiba, Japan).

2.3. Cell culture experiment

The human osteoblast-like cells (MG-63 cell, Cell bank, Shanghai, China) were used and cultured in the Dulbecco's modified Eagle's medium (DMEM). Ionic extracts were first prepared by immersing each group of powders in DMEM culture medium with concentration of 100 mg/ml. After incubation at 37 °C for 24 h, the mixture was centrifuged and the supernatant was collected. Subsequently, these extracts were sterilized by filtration through 0.22 μm filter membrane for cell culture experiments. The ion concentrations of the extracts were measured by ICP-OES (Optima 8000, PerkinElmer, USA). The proliferation of MG-63 was carried out using Cell Counting Kit-8 (CCK-8) assay at

a density of 5×10^3 cells/96-well for 1 and 3 days of culture by the method reported previously [10]. The results were expressed as optical density (OD) and all experiments were done in triplicate to obtain the average data.

III. Results and discussion

3.1. The effect of urea concentration

It is well known that with the increase of the hydrothermal temperature urea ($(NH_2)_2CO$) in the reaction system continuously decomposes to form CO_2 and aqueous ammonia species (NH_3). The released NH_3 easily dissolves in water and increases the pH value to alkaline condition, wherein HA becomes the more thermodynamically stable compound. Therefore, the continuous and homogeneous decomposition of urea generates the driving force for the nucleation and growth of HA crystals under moderate supersaturation conditions. In addition, CO_2 dissolves in water and then incorporates as carbonate in the HA lattice [16].

Figure 1 presents XRD patterns of the FHA porous microspheres with different urea concentrations. All of the products were identified as pure HA phase without other impurities. With the increase of urea concentration, the peak corresponding to (112) plane gradually disappeared and finally it overlapped with the (211) peak to form a broad peak. With the increase of urea concentration, the more and more CO_3^{2-} produced by the decomposition of urea entered the apatite structure, causing the disordered lattice [17]. As a result, the crystallinity of the hydrothermally synthesized FHA porous microspheres decreased from 81.4% to 71.7%.

CO_3^{2-} in HA has two alternative types named as A-type and B-type. In the former CO_3^{2-} replaces OH^- and in the latter CO_3^{2-} replaces PO_4^{3-}. Substitution types have different effects on the lattice parameters of HA. Studies have shown that B-type substitution will cause the lattice parameter *a* to decrease and *c* to increase [18], whereas A-type substitution will cause the lattice parameter *c* to decrease [19]. It can be seen from Table 1 that the lattice parameter *a* decreased, the *c* rose first and then descended with the increase of urea concentration, indicating that the obtained products in hydrothermal conditions were carbonated HA giving priority to B-type substitution. As the urea concentration further increased, more CO_2 generated by decomposition promoted carbonate substitution, and the possibility of A-type substitution also increased. Previous studies [20] have shown that the presence of B-type carbonate in the apatite will interfere with the apatite crystallization and which then tends to form small-size crystals, which can explain our XRD and SEM results well.

Figure 2 presents SEM images of the FHA microspheres prepared with different urea concentrations. It can be seen from Fig. 2a that only parts of crystals assembled into microspheres with a large number of rod-like crystals being scattered randomly. The crystals in the samples U2 and U3 grew into nanosheets, whereas the more inhomogeneous and smaller rod-like structures appeared in the sample U4. Almost all crystals of the sample U2 were successfully assembled into spheres and the loose and porous microsphere structure can be clearly observed in the enlarged image (Fig. 2b). All of the formed microspheres in the sample U3 exhibited good dispersion without obvious agglomeration (Fig. 2c). With the further increase in urea concentration, the obtained microspheres were characterized by uneven size and irregular morphology (Fig. 2d).

According to the Gibbs free energy change [21], the larger the supersaturation is, the more free energy of crystal growth goes down and the crystal nucleus can rapidly precipitate in the solution and grow into nanocrystals in the early stage. Due to the high surface energy, the as-formed nanocrystals aggregated to reduce their surface energy in solution. The optimum shape for minimizing the surface free energy is a spherical structure due to the lowest surface area of the spheres, which favours the self-assembling of the 2D nanocrystals into microspheres rather than other types of aggre-

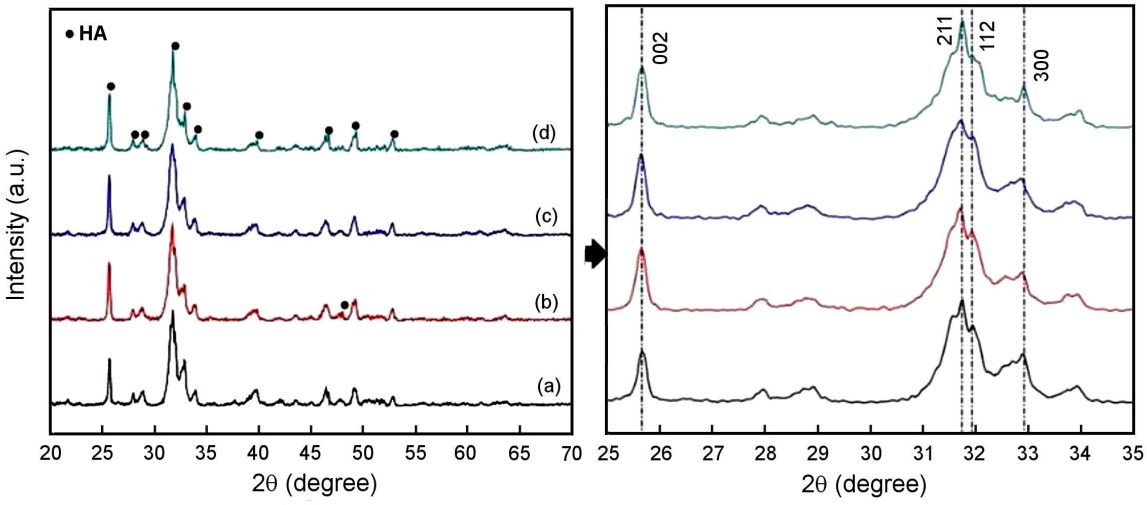

Figure 1. XRD patterns of the FHA samples with different urea concentrations: a) U1, b) U2, c) U3 and d) U4

Table 1. The effect of different urea concentration on lattice parameters and diffraction angle

Sample	Lattice constant		2θ [°]		Crystallinity [%]
	a [Å]	c [Å]	(002)	(300)	
U1	9.425	6.927	25.69	32.87	81.4
U2	9.410	6.934	25.66	32.85	80.2
U3	9.409	6.936	25.65	32.80	78.4
U4	9.406	6.928	25.68	32.91	71.7

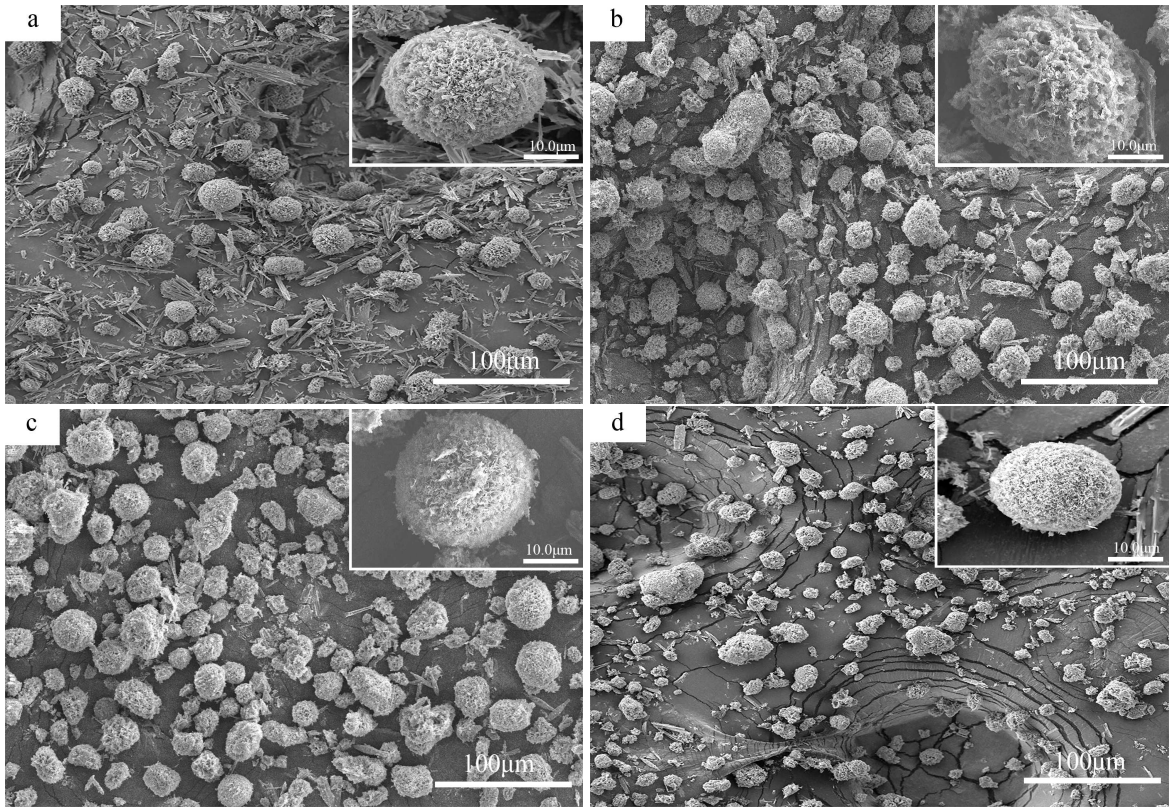

Figure 2. SEM images of samples with different urea concentrations: a) U1, b) U2, c) U3 and d) U4

gations [22]. The increase of pH and supersaturation caused by the urea hydrolysis in the hydrothermal process can effectively promote the formation of HA microspheres. Due to the low urea concentration of the sample U1, the low supersaturation made the driving force towards nucleation insufficient. It tended to form of larger rod-like crystals, which was difficult to assemble into a sphere. The supersaturation provided by the urea hydrolysis in the samples U2 and U3 can coordinate the nucleation and growth of HA crystals, thus crystal grew into nanosheets with a tendency to assemble as "petals" into porous microspheres structure. However, the excessively urea concentration in the sample U4 increased the supersaturation too much, which led to faster nucleation and smaller crystals. Rapid microsphere self-assembly process made the assembled microspheres small and dense.

Figure 3 shows N_2 adsorption/desorption isotherms and BJH pore size distribution curves of the FHA microspheres prepared with different urea concentrations. All the samples have similar type IV adsorption/desorption isotherms and the typical H3-hysteresis loops [23] deriving from particles aggregates with silt-shaped pores [24]. With the continuous increase of urea concentration from 0.75, to 1.25 mol/l, the specific surface area (S_{BET}) increased from 46.8 to 91.8 m^2/g and pore volume (V_p)

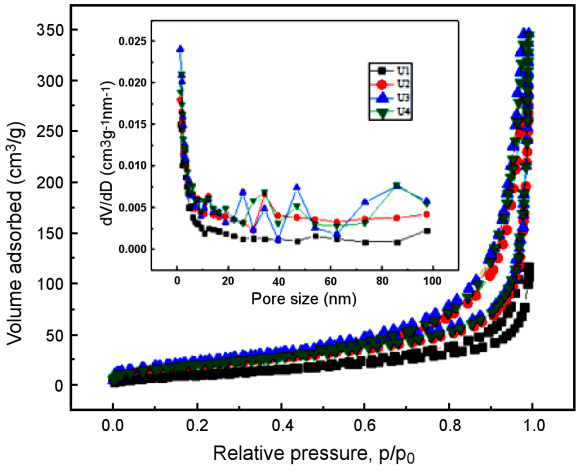

Figure 3. The nitrogen adsorption curves and pore size distributions of FHA microspheres with different urea concentrations

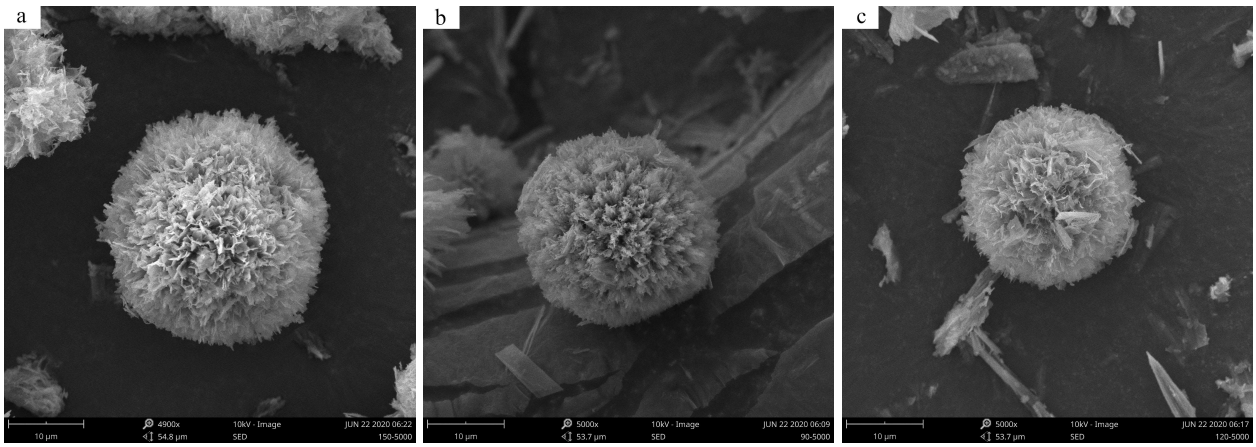

Figure 4. SEM images of the U3 synthesized at different hydrothermal temperatures: a) 90 °C, b) 120 °C and c) 150 °C

Table 2. The effect of different urea concentrations on the specific surface area S_{BET}, pore volume V_p and average pore size D

Sample	S_{BET} [m^2/g]	V_p [cm^3/g]	D [nm]
U1	46.8	0.18	10.39
U2	75.4	0.43	22.86
U3	91.8	0.53	25.68
U4	76.1	0.52	20.45

also increased from 0.18 to 0.53 cm^3/g, respectively (Table 2). However, due to the dense structure of the formed microspheres, the S_{BET} of the sample U4 decreased to 76.1 m^2/g instead. Moreover, the increasing number of mesopores indicated the wider distribution of pore sizes and the more complex pore structure. The characteristics such as high S_{BET}, large V_p and complex porous structure not only provided ideal physical space, active adsorption sites and nanoscale channels for the loading and sustained release of traditional drugs, but also made conditions for the *in situ* adsorption and sustained release of carrier ions.

3.2. The effect of hydrothermal temperature

Morphologies of the FHAs obtained at different hydrothermal temperatures are shown in Fig. 4. When the hydrothermal temperature was 90 °C, the FHA microspheres self-assembled from small acicular crystals into dandelion clusters with compact structure. At the temperature of 120 °C, the flaky crystals self-assembled into porous flower-like microspheres. When the hydrothermal temperature increased to 150 °C, the microspheres tended to be uniform and compact with fully-developed flaky crystal. With the increase of temperature, urea hydrolysed more quickly to induce the ion concentration higher than required for crystal nucleation in solution. Then the rapid outbreak of homogeneous nucleation effect made ion concentration to drop sharply and the formed nanoparticles lost the nutritional conditions for continuous growth. As a result, the obtained particles can be controlled within the small size range. The morphology observation showed that the fabricated FHA porous microspheres with diameters of about 30 μm were assembled from two-dimensional nanosheets with 30–70 nm in thickness, up to 4–5 μm in length and about 2 μm in width. Under the different condition of hydrothermal temperatures, the different driving forces of nucleation and growth induced formation of different morphology and size of crystals, leading to different microsphere structures.

Figure 5 shows the nitrogen adsorption curve and BJH pore size distribution of the U3 microspheres prepared at different hydrothermal reaction temperatures. With the increase of the reaction temperature from 90 to 120 °C, the specific surface area and pore volume increased from 58.6 to 75.4 m^2/g and from 0.31 to 0.43 cm^3/g, respectively (Table 3). However, when the temperature rose to 150 °C, both the specific surface area and pore volume decreased a little bit, which were consistent with the phenomenon that the microspheres formation tended to be uniform and compact as observed in Fig. 4c.

It is well known that the substitution process of fluorine into apatite lattice was controlled by the diffusion of fluoride ion and the formation of fluoride-containing apatite [25]. The increase of temperature will increase the

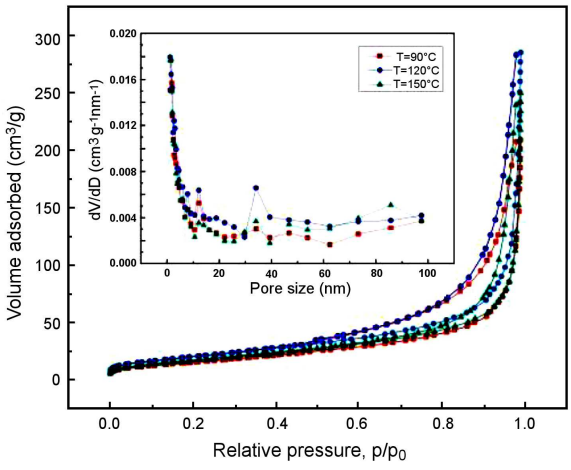

Figure 5. The nitrogen adsorption curves and pore size distributions of U3 synthesized at different hydrothermal temperatures

Table 3. The effect of different hydrothermal temperatures on pore structure parameters and fluorine contents C_F

Temperature [°C]	S_{BET} [m^2/g]	V_p [cm^3/g]	C_F [wt.% apatite]
90	58.6	0.31	0.414
120	75.4	0.43	0.675
150	66.7	0.38	0.814

diffusion coefficient and promote the formation of FHA. As a result, the fluoride contents of the FHA increased from 0.414 to 0.814 wt.% in apatite with the hydrothermal temperature, as listed in Table 3.

3.3. F^- release properties

The data obtained from the fluoride ion release studies are displayed in Fig. 6. Obvious burst of fluoride release can be observed in the sample U1, and the overall fluoride release data fluctuated greatly, indicating the poor stability of the fluoride release. The reason may be related to the large number of scattered rod-like crystals existing in the sample U1, characteristic of fewer microspheres, small S_{BET} and low V_p. The rapid dissolution and release of F^- in physiological salt solution resulted in a burst of fluoride concentration on the first day. When F^- is released from the crystal, the positively charged Ca^{2+} could form strong adsorption site. As a result, the released F^- would re-enter the apatite in the form of chemical adsorption and physical adsorption, which slowed down the F^- release to a certain extent within 6 days. However, when the concentration of F^- in the solution was too low, adsorbed F^- on the surface was quickly released under the driving force of the concentration difference, which caused another burst of F^- release on the 9th day. With the dynamic process of adsorption-desorption, F^- concentration fluctuated during the soaking time. The released F^- concentration of the sample U2 was stably maintained in the range of 95–190 μg/l (the therapeutic window of serum F^-) within 30 days, which could well fulfil the requirements of fluoride release carriers. When the U2 microspheres were

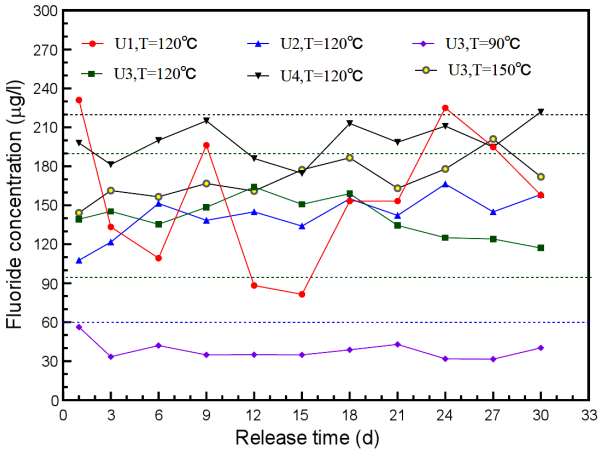

Figure 6. Fluoride release curves of FHA microspheres with different urea concentrations

immersed in physiological salt solution, the F^- on the surface of the microsphere dissolved first, so the F^- concentration increased in the first few days, and then the F^- ions inside the microspheres were also gradually dissolved and released with time. Due to the complex pore structure of the microspheres and the messy pore size distribution, the release path for F^- ions was definitely prolonged. It can be seen from Table 2 that the obtained microsphere had higher V_p, indicating more surface active sites which can adsorb the released F^- in order to avoid the accumulation of F^- in the solution. The fluoride-releasing process of the sample U3 was similar to that of the sample U2. Larger S_{BET} of the sample U3 indicated more complex pore structure, which will significantly extend the release path of F^-. In the same way, the increase in V_p can help adsorb more F^- so as to maintain F^- in a lower range. Therefore, its average released fluoride concentration was lower and more stable. The fluoride-releasing concentrations of the sample U4 during 30 days were also relatively stable, but it exceeded the range of fluoride therapy. The increase of urea concentration promoted the carbonate substitution, which led to higher solubility of FHA and then F^- ions dissolved and released more quickly, inducing the average fluoride release concentration of about 200 μg/l. However, due to the large V_p and S_{BET} of the microsphere structure, the released fluoride concentration of the sample U4 was guaranteed to maintain at high and stable level.

Fluoride ion releases of the U3 samples synthesized at different hydrothermal temperatures were relatively stable. The burst release on the first day indicated the ions release from the surface of the microspheres in physiological salt solution, while the subsequent stable release within a certain range can be attributed to the pore size and pore structure of the microspheres. As shown in Fig. 4a, the structure of the microspheres obtained at 90 °C was relatively dense with small average pore size, which would extend the release path of F^- and reduce the release rate to a certain extent. Because the fluoride load of the microspheres obtained at 90 °C was only 0.414 wt.% in apatite, correspondingly, the F^- concentration was only stably maintained in the range of 30–60 μg/l within 30 days, which is higher than that in the body fluid of normal adult humans (7.2–43.7 μg/l) [6]. The fluoride-releasing concentration of the microspheres synthesized at 120 °C was stable in the therapeutic range (95–190 μg/l), which was attributed to the good microsphere formation, the complex pore structure, and the large S_{BET} and pore volume. The average fluoride-releasing concentration of the samples prepared at 150 °C was much higher due to the high fluoride loading.

3.4. Cell culture of FHA porous microspheres

The ICP-OES analysis indicated that F^- ion concentrations of the extracts for cell culture were 0.072, 0.073, 0.075 and 0.082 mmol/l for the samples U1, U2,

U3 and U4, respectively. The B-type CO_3^{2-} substitution promoted by the decomposition of urea decreased the crystallinity. As a result, the dissolution rate of the FHA samples can be expected as U4 > U3 > U2 > U1. No significant difference on F^- ion concentrations of the extracts for the samples U1, U2 and U3 can be detected due to their similar structure and crystallinity. On the other hand, the excessive urea concentration of the sample U4 decreased the crystallinity to 71.7%, which promoted the extraction of F^- ions. Moreover, with the increase of hydrothermal temperature, F^- ion concentrations of the U3 extracts for cell culture increased from 0.046 mmol/l (90 °C) to 0.085 mmol/l (150 °C), which were consistent with the change trend of fluoride content of the FHA porous microspheres seen in Table 3.

Many researchers have also demonstrated that fluoride ions in the culture medium stimulated osteoblastic activities in terms of cell proliferation and differentiation [26]. For example, Cheng *et al.* [27] reported that FHA with fluoride content in the range 0.033–0.4 mol F/mol was suitable for implantation. Wang *et al.* [28] indicated that coatings with fluoride contents in range 0.8–1.1 had a stronger stimulating effect on cell proliferation and differentiation activities. However, high F^- concentration in bone can also lead to severe adverse effects such as osteomalacia [29].

The CCK-8 evaluation results revealed that all extracts of the FHA porous microspheres exhibited no cytotoxicity to MG-63, as shown in Fig. 7. There was no significant difference in the fabricated FHA samples after being incubated for 1 day. A greater proliferation rate occurred after 3 days of culture. The OD values of the ionic product from the porous U3 microspheres prepared at 120 °C on MG-63 proliferation was extraordinarily higher than other materials in culture periods, which was attributed to optimal F^- ion concentrations. Too high F^- ion concentration of samples with exorbitant solubility and fluoride contents may interfere with the stimulatory effect on cell proliferation. So, the capability of tailoring the solubility and microstructure of the FHA microsphere is quite useful for the long-term controllable F^- releasing properties.

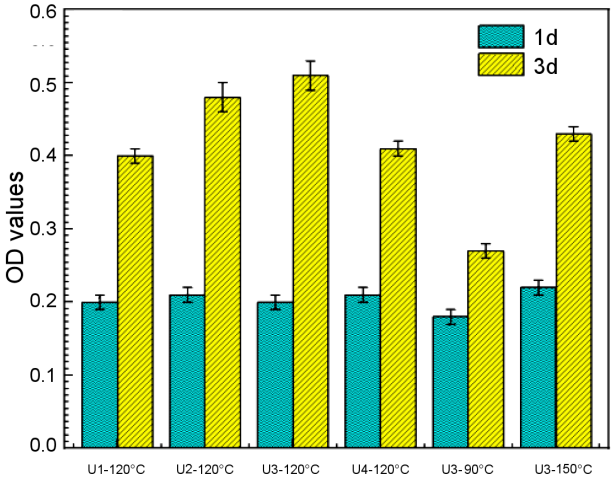

Figure 7. The effect of dissolved products from FHA porous microspheres on proliferation of MG-63 after culturing for 1 and 3 days

IV. Conclusions

In the absence of any template-directing reagents, porous fluoride-substituted hydroxyapatite microspheres were successfully synthesized by hydrothermal method as the carrier for *in situ* controlled fluoride release. The ideal structure of microspheres can be obtained by regulating urea concentration (1–1.25 mol/l) and hydrothermal temperature (120–150 °C). The synthesized FHA microspheres in diameters of about 30 μm with large specific surface area (75.4–91.8 m^2/g), large pore volume (0.43–0.53 cm^3/g) and complex porous structure were helpful for the adsorption and long-term stable release of ionic extracts. The ionic product of the FHA porous microspheres could apparently stimulate the proliferation of MG-63 at certain concentrations of F^- ion. F^- concentration in physiological salt solution was maintained in the range of the therapeutic window (95–190 μg/l) without exceeding the toxic threshold within 30 days, which may be a potential candidate as bioactive fluoride-release carrier for the treatment of osteoporosis and bone defects.

Acknowledgements: The authors gratefully acknowledge financial support from the Natural Science Foundation of Tianjin China (Grant No. 19JCZDJC37800), the Science and Technology Plans of Tianjin China (Grant No. 20YDTPJC01690), Innovation and entrepreneurship projects of college students (Grant No. 202210058154).

References

1. L. Tammaro, V. Vittoria, A. Calarco, O. Petillo, F. Riccitiello, G. Peluso, "Effect of layered double hydroxide intercalated with fluoride ions on the physical, biological and release properties of a dental composite resin", *J. Dentistry*, **42** [1] (2014) 60–67.
2. X. Luo, D. Barbieri, G. Passanisi, H. Yuan, J.D. Bruijn. "Influence of fluoride in poly(D,L-lactide)/apatite composites on bone formation", *J. Biomed. Mater. Res.: Part B Appl. Biomater.*, **103** [4] (2014) 841–852 .
3. N.P. Chau, S. Pandit, J.E. Jung, J.N. Cai, H.K. Yi, J.G. Jeon, "Long-term anti-cariogenic biofilm activity of glass ionomers related to fluoride release", *J. Dentistry*, **47** (2016) 34–40.
4. H.B. Li, F. Jiang, S. Ye, Y.Y. Wu, K.P. Zhu, D.P. Wang, "Bioactive apatite incorporated alginate microspheres with sustained drug-delivery for bone regeneration application", *Mater. Sci. Eng. C*, **62** (2016) 779–786.
5. G.M. Keegan, J.D. Smart, M.J. Ingram, L.M. Barnes, G.R. Burnett, G.D. Rees, "Chitosan microparticles for the controlled delivery of fluoride", *J. Dentistry*, **40** (2012) 229–240.
6. Y. Sogo, A. Ito, D. Yokoyama, A. Yamazaki, R.Z. LeGeros, "Synthesis of fluoride-releasing carbonate apatites for bone substitutes", *J. Mater. Sci. Mater. Med.*, **18** (2007)

1001–1007.
7. J. Liu, S.C.F. Rawlinson, R.G. Hill, F. Fortune, "Fluoride incorporation in high phosphate containing bioactive glasses and in vitro osteogenic, angiogenic and antibacterial effects", *Dental Mater.*, **32** (2016) 221–237.
8. M. Kheradmandfard, M.H. Fathi, M. Ahangarian, E. Mohammadi Zahrani, "In vitro bioactivity evaluation of magnesium-substituted fluorapatite nanopowders", *Ceram. Int.*, **38** (2012) 169–175.
9. M.H. Ghaemi, S.Y. Sayenko, V. Shkuropatenko, A. Zykova, K. Ulybkina, O. Bereznyak, A. Krupa, M. Sawczak, "The effect of Sr and Mg substitutions on structure, mechanical properties and solubility of fluorapatite ceramics for biomedical applications", *Process. Appl. Ceram.*, **16** (2022) 218–229.
10. K.L. Lin, P.Y. Liu, L. Wei, Z.Y. Zou, W.B. Zhang, Y. Qian, Y.H. Shen, J. Chang, "Strontium substituted hydroxyapatite porous microspheres: Surfactant-free hydrothermal synthesis enhanced biological response and sustained drug release", *Chem. Eng. J.*, **222** (2013) 49–59.
11. C. Qi, Y.J. Zhu, B.Q. Lu, "Hydroxyapatite nanosheet-assembled porous hollow microspheres: DNA-templated hydrothermal synthesis, drug delivery and protein adsorption", *J. Mater. Chem.*, **22** (2012) 22642–22650.
12. J. Yao, H. Wu, Y.L. Ruan, ""Reservoir" and "barrier" effects of ABC block copolymer micelle in hydroxyapatite mineralization control", *Polymer*, **52** (2011) 793–803.
13. H. Yang, H. Li, "Preparation and sustained-release properties of porous hydroxyapatite hollow microspheres", *J. Synth. Cryst.*, **42** (2013) 2412–2417.
14. J.S. Xu, Y.J. Zhu, "C-Fe_2O_3 and Fe_3O_4 magnetic hierarchically nanostructured hollow microspheres: preparation, formation mechanism, magnetic property, and application in water treatment", *J. Colloid Interface Sci.*, **385** (2012) 58–65.
15. I.S. Neira, Y.V. Kolen'ko, O.I. Lebedev, G. Van Tendeloo, H.S. Gupta, F. Guitián, M. Yoshimura, "An effective morphology control of hydroxyapatite crystals via hydrothermal synthesis", *Cryst. Growth Des.*, **9** [1] (2009) 466–474.
16. S.P. Parthiban, I.Y. Kim, K. Kikuta, C. Ohtsuki, "Effect of urea on formation of hydroxyapatite through double-step hydrothermal processing", *Mater. Sci. Eng. C*, **31** (2011) 1383–1388.
17. Q.X. Zhu, J.Q. Wu, "Effective factors of preparation for carbonated hydroxyapatite by the aqueous precipitation method", *J. Chin. Ceram. Soc.*, **35** [6] (2007) 690–695.
18. F.Z. Ren, X. Lu, Y. Leng, "Ab initio simulation on the crystal structure and elastic properties of carbonated apatite", *J. Mech. Behav. Biomed. Mater.*, **26** (2013) 59–67.
19. S. Jebri, H. Boughzala, A. Bechrifa, M. Jemal, "Structural analysis and thermochemistry of "A" type phosphostrontium carbonate hydroxyapatites", *J. Therm. Anal. Calorim.*, **107** (2011) 963–972.
20. C.C. Kee, H. Ismail, A.F. Mohd Noor, "Effect of synthesis technique and carbonate content on the crystallinity and morphology of carbonated hydroxyapatite", *J. Mater. Sci. Technol.*, **29** [8] (2013) 761–764.
21. K.C. Zhang, L.Q. Zhang, *Crystal Growth*, Science Press, Beijing, China, 1981.
22. D. Vanmaekelbergh, "Self-assembly of colloidal nanocrystals as route to novel classes of nanostructured materials", *Nano Today*, **6** (2011) 419–437.
23. Y.P. Guo, Y.B. Yao, Y.J. Guo, C.Q. Ning, "Hydrothermal fabrication of mesoporous carbonated hydroxyapatite microspheres for a drug delivery system", *Micropor. Mesopor. Mater.*, **155** (2012) 245–251.
24. Y.J. Guo, Y.Y. Wang, T. Chen, Y.T. Wei, L.F. Chu, Y.P. Guo, "Hollow carbonated hydroxyapatite microspheres with mesoporous structure: Hydrothermal fabrication and drug delivery property", *Mater. Sci. Eng. C*, **33** [6] (2013) 3166–3172.
25. Q.X. Zhu, W.H. Jiang, H.D. Wang, "Investigation on preparation factors for fluorhydroxyapatite by an aqueous precipitation method", *J. Inorg. Mater.*, **26** [12] (2011) 1345–1340**.**
26. J. Harrison, A.J. Melville, J.S. Forsythe, B.C. Muddle, A.O. Trounson, K.A. Gross, R. Mollard, "Sintered hydroxyfluorapatites - IV: The effect of fluoride substitutions upon colonisation of hydroxyapatites by mouse embryonic stem cells", *Biomaterials*, **25** (2004) 4977–4986.
27. K. Cheng, W. Weng, H. Wang, S. Zhang, "In vitro behavior of osteoblast-like cells on fluoridated hydroxyapatite coatings", *Biomaterials*, **26** (2005) 6288–6295**.**
28. Y.S. Wang, S. Zhang, X.T. Zeng, L.L. Ma, W. Weng, W. Yan, M. Qian, "Osteoblastic cell response on fluoridated hydroxyapatite coatings", *Acta Biomater.*, **3** (2007) 191–197
29. H.B. Qu, M. Wei, "The effect of fluoride contents in fluoridated hydroxyapatite on osteoblast behaviour", *Acta Biomater.*, **2** (2006) 113–119.